

Effect of Filler and Void to the Shear Properties of Pultruded Composites

by
Jin Y. Park, Department of Mechanical and Civil
Engineering, Minnesota State University, Mankato, MN
USA

ABSTRACT

This study presents the results of an analytical investigation aimed at examining the mechanical behavior of fiber-reinforced pultruded composites containing nonhomogeneous constituents such as fine clay fillers under shear loading. Analytical formulae that account for the presence of inhomogeneities in the matrix materials were developed for estimating the extensional and in-plane shear moduli, and Poisson's ratio. The analytical results were compared with the properties obtained from experiments. For the experiments, the pultruded composites containing clay fillers and voids as well as E-glass fibers and vinyl ester resin were selected, analyzed and tested under shear loading. The effects of presence of constituents on the mechanical properties of matrix materials were also investigated based on the obtained volume fraction of their constituents.

INTRODUCTION

Micromechanical analytical models can serve as a guide for engineers in establishing mechanical properties during both the manufacturing stage and preliminary design. Although some of the mechanical properties (such as extensional and shear moduli) of polymer composite materials can be determined by physical experiments, the experiments cannot be performed before the fabrication. Since the specific configuration must have been made prior to testing, it is usually time consuming and costly to repeat fabrications and testings to have a specific composite material. Therefore, the development of an analytical model for the prediction of mechanical properties of polymer composites based on their micromechanical constituents and structures is very useful to composite manufacturers.

Pultruded polymer composites usually consist of roving and CSM (Continuous Strand Mat), polymer resin, fillers (micro/nano particles), a small amount of catalyst, and unwanted voids (porosity). The filler acts as a resin extender and reduces porosity in the surface of the polymer composites. The particle size of the filler is an

important design characteristic, as smaller particles will absorb more resin on the surface and tend to increase the resin mix viscosity. It is also known that the filler with smaller size can reinforce polymer composites in great deal.

The objective of this study was to develop analytical evaluation methods that permit the estimation of the mechanical properties of pultruded composites with considering the shapes and volume fractions of filler and void. The mechanical properties were predicted theoretically by micromechanical studies. The micromechanical studies included the measurements of volume fractions of the composite constituents. Park [1] proposed three micromechanical models of polymer composite materials containing 3-D spherical inhomogeneities and showed the validity of the evaluation by comparison with experimental results.

There are a number of analytical models that can be used for predicting the macromechanical properties of pultruded composite materials. However, few attempts have been made to evaluate the properties of pultruded composites with considering filler and void contents. In this study, the matrix is treated as an isotropic medium containing platelet clay fillers and the voids whose shapes are closed to ellipsoid. The isotropic medium with clay fillers was evaluated by using a platelet filler model. This filler models will be discussed in the following sections. The matrix containing voids was analyzed by the modified Mori-Tanaka model [1-4]. Reviews and modifications of all of these methods were performed by Mura [5] and Park. For experimental program, three pultruded polymer composites specimen groups were prepared and tested under a shear loading.

ANAYTICAL MODELS

Clay Particle

The typical clay particle has a hexagonal platelet shape [6] as shown in Fig. 1. The single crystal of clay is a two layer hydrous alumino silicate, consisting of chemically bounded layers of silica and hydrous alumina. The majority of clay particles in the composite materials under consideration had 0.4-6.0 μm (400-6,000 nm) diameter (equivalent diameter of a circle of the same area). Based on diameters, the materials are not quite nanocomposites. The aspect ratios between thickness t and diameter d (Fig. 1) of the clay particles are in the range of 1/100-1/10, so that their thicknesses are in the range of 4-600 nm. The thickness of the clay particles have nano-dimensions. Therefore, the materials in this study were considered as micro/nanocomposites.

Micromechanical Modeling of an Isometric Resin Matrix with Platelet Fillers

Unidirectional Model

Figure 2 shows the schematic micromechanical figures of the mixture of unidirectional clay fillers with the matrix. This theoretical model shown in Fig. 2a does not represent a realistic matrix structure, but should be used to obtain the properties of the mixture of resin matrix and randomly oriented and evenly distributed clay fillers shown in Fig. 2b. The 1- and 2-axes of each particle in Fig. 2a coincide with the x - and y -axes in the global coordinate system. Since it is assumed that the unidirectional particles are distributed evenly in the matrix, the mechanical properties of the matrix shown in Fig. 2a are identical along the x - and y - axes. Therefore, this is a transversely isotropic material. Considering the properties of the transversely isotropic materials shown in Fig. 2a ($E_{xx}^0 = E_{yy}^0$, $G_{zx}^0 = G_{yz}^0$, $\nu_{xz}^0 = \nu_{yz}^0$, $\nu_{zx}^0 = \nu_{zy}^0$), the transversely isotropic material has stress-strain relations as follows:

$$\begin{Bmatrix} \sigma_{xx}^0 \\ \sigma_{yy}^0 \\ \sigma_{zz}^0 \\ \tau_{yz}^0 \\ \tau_{zx}^0 \\ \tau_{xy}^0 \end{Bmatrix} = \begin{bmatrix} C_{11}^0 & C_{12}^0 & C_{13}^0 & 0 & 0 & 0 \\ C_{12}^0 & C_{11}^0 & C_{13}^0 & 0 & 0 & 0 \\ C_{13}^0 & C_{13}^0 & C_{33}^0 & 0 & 0 & 0 \\ 0 & 0 & 0 & C_{44}^0 & 0 & 0 \\ 0 & 0 & 0 & 0 & C_{44}^0 & 0 \\ 0 & 0 & 0 & 0 & 0 & C_{66}^0 \end{bmatrix} \begin{Bmatrix} \varepsilon_{xx}^0 \\ \varepsilon_{yy}^0 \\ \varepsilon_{zz}^0 \\ \gamma_{yz}^0 \\ \gamma_{zx}^0 \\ \gamma_{xy}^0 \end{Bmatrix} \quad (1)$$

where

$$\begin{aligned} C_{11}^0 &= \frac{1 - \nu_{xz}^0 \nu_{zx}^0}{E_{xx}^0 E_{zz}^0 \Delta}; & C_{33}^0 &= \frac{1 - \nu_{xy}^0 \nu_{yx}^0}{(E_{xx}^0)^2 \Delta} \\ C_{12}^0 &= \frac{\nu_{yx}^0 - \nu_{xz}^0 \nu_{zx}^0}{E_{xx}^0 E_{zz}^0 \Delta}; & C_{13}^0 &= \frac{\nu_{xz}^0 - \nu_{xy}^0 \nu_{xz}^0}{(E_{xx}^0)^2 \Delta} \\ C_{44}^0 &= G_{zx}^0; & C_{66}^0 &= G_{xy}^0 \\ \Delta &= \frac{1 - \nu_{xy}^0 \nu_{yx}^0 - 2\nu_{xz}^0 \nu_{zx}^0 - 2\nu_{yx}^0 \nu_{xz}^0 \nu_{zx}^0}{(E_{xx}^0)^2 E_{zz}^0} \end{aligned} \quad (2)$$

where $[C^0]$ is the stiffness matrix of a transversely isotropic material and C_{ij}^0 are its components. C_{66}^0 can be replaced by $(C_{11}^0 - C_{12}^0)/2$.

Micromechanical Modeling for Obtaining C_{ij}^0

This section presents the procedure to obtain the components of stiffness matrix of the mixture of resin, voids and unidirectional platelet fillers (C_{ij}^0). The Modified Mori-Tanaka model presented in Park [1] were used to evaluate the shear and bulk moduli of the resin matrix containing voids without fillers (G_{r+v} and K_{r+v} , respectively) can be obtained.

$$G_{r+v} = G_r \left\{ 1 - \frac{\nu_{void/m}}{(1 - 2S_{1212})\nu_{r/m}} \right\} \quad (3)$$

$$K_{r+v} = K_r \left\{ 1 - \frac{3\nu_{void/m}}{(3 - S_{kkll})\nu_{r/m}} \right\} \quad (4)$$

and

$$\begin{aligned} S_{1212} &= \frac{3K_r + 6G_r}{15K_r + 20G_r} \\ S_{kkll} &= \frac{9K_r}{3K_r + 4G_r} \end{aligned} \quad (5)$$

where where $\nu_{r/m}$ is the volume fraction of the resin in the matrix. Note that $\nu_{r/m} + \nu_{filler/m} + \nu_{void/m} = 1$. S_{ijkl} is Eshelby's tensor for spherical inclusions [5]. Randomly oriented and evenly distributed ellipsoidal voids can be assumed as spherical inclusion in the matrix [1]. From Eq. (3), G_r is the shear modulus of polymer resin. $\nu_{void/m}$, and $\nu_{r/m}$ are the volume fractions of void and polymer resin in the matrix, respectively. From Eq. (4), K_r is the bulk modulus of polymer resin.

Young's modulus of the resin matrix containing voids is computed from the shear and bulk moduli using the following relation:

$$E_{r+v} = \frac{9K_{r+v}}{1 + 3K_{r+v}/G_{r+v}} \quad (6)$$

Let G_{xy}^0 denote the shear moduli of the mixture of an isometric resin, unidirectional platelet fillers and voids (Fig. 2a) obtained by using micromechanical models. The magnitude of G_{xy}^0 is obtained from the Modified Mori-Tanaka model:

$$G_{xy}^0 = G_{r+v} \left\{ 1 + \frac{\nu_{filler/m}(G_{filler} - G_{r+v})}{G_{r+v} + 2S'_{1212}(\nu_{r/m} + \nu_{void/m})(G_{filler} - G_{r+v})} \right\} \quad (7)$$

where

$$S'_{1212} = \frac{3\pi}{64} \left(\frac{3K_{r+v} + 5G_{r+v}}{3K_{r+v} + 4G_{r+v}} \right) \quad (8)$$

The Halpin-Tsai [7] theory is the approximated form of generalized Self-consistent micromechanical model. The elastic properties of unidirectional discontinuous reinforcement (such as the unidirectional model shown in Fig. 2a) can be obtained using the Halpin-Tsai equations:

$$\begin{aligned}
E_x^0 = E_y^0 &= \frac{1 + 2\eta_T \nu_{filler/m}}{1 - \eta_T \nu_{filler/m}} E_{r+v} \\
E_z^0 &= \frac{1 + 2S_p \eta_L \nu_{filler/m}}{1 - \eta_L \nu_{filler/m}} E_{r+v} \\
G_{zx}^0 = G_{zy}^0 &= \frac{1 + 2\eta_G \nu_{filler/m}}{1 - \eta_G \nu_{filler/m}} G_{r+v} \\
\nu_{zx}^0 = \nu_{zy}^0 &= \nu_{filler} \nu_{filler/m} + \nu_r \nu_{r/m}
\end{aligned} \tag{9}$$

and

$$\begin{aligned}
\eta_T &= \frac{E_{filler} / E_{r+v} - 1}{E_{filler} / E_{r+v} + 2} \\
\eta_L &= \frac{E_{filler} / E_{r+v} - 1}{E_{filler} / E_{r+v} + 2S_p} \\
\eta_G &= \frac{G_{filler} / G_{r+v} - 1}{G_{filler} / G_{r+v} + 1}
\end{aligned} \tag{10}$$

where E_x^0 , E_y^0 and E_z^0 are the extensional moduli of the mixture of unidirectional platelet fillers and resin matrix in the x -, y - and z -directions, respectively (see Fig. 2a). G_{zx}^0 ($=G_{xz}^0$) and G_{zy}^0 ($=G_{yz}^0$) are shear moduli of the mixture in the zx - and yz -planes, respectively. ν_{zx}^0 and ν_{zy}^0 are poisson's ratios of the mixture in the zx - and yz -planes, respectively. S_p is the ratio of the average thickness and diameter of fillers.

The Poisson's ratio in the xy -plane, ν_{xy}^0 can be also obtained using the following relation of transversely isotropic materials:

$$\nu_{xy}^0 = \frac{E_x^0}{2G_{xy}^0} - 1 \tag{11}$$

Since E_x^0 and G_{xy}^0 are known, ν_{xy}^0 can be computed from Eq. (11). The components of the stiffness matrix C_{11}^0 , C_{12}^0 , C_{13}^0 , C_{33}^0 , C_{44}^0 , C_{66}^0 are computed by using Eq. (2).

Randomly Oriented Olay Fillers about the x -axis

The next step is to obtain the mechanical properties of the matrix with randomly oriented and evenly distributed fillers in it (Fig. 2b). The unidirectional filler model (Fig. 2a) of the mixture of fillers and isotropic resin is now rotated by an angle q about the x -axis. By using the stiffness matrix of the mixture of unidirectional platelet fillers and polymer matrix [C^0] and a transformation

matrix about the x -axis [T_x], the transformed stiffness matrix [C'] can be computed:

$$[C'] = [T_x][C^0][T_x]^T \tag{12}$$

where [T_x]^T is the transpose matrix of [T_x].

According to classical laminate theory, the in-plane strains are uniform throughout the thickness under in-plane loadings. Thus, the mixture of randomly rotated fillers along the x -axis and the isotropic matrix can be treated as laminated layers with unidirectional lamina in every direction. It is also noted that each lamina must be thicker than the widths of the fillers. The effective stiffnesses, \bar{C}'_{ij} are obtained by summing the plane stress moduli through the thickness in proportion to the percentage of the thickness of the k th lamina in the n -ply laminate:

$$\bar{C}'_{ij} = \frac{1}{t} \sum_{k=1}^n C'_{ij}{}^{(k)} t_k = \frac{1}{\pi} \int_0^\pi C'_{ij} d\theta \tag{13}$$

where t_k is the thickness of the k th lamina and t is the total thickness of the laminate.

3-D randomly Oriented Clay Fillers in the Matrix

Another rotation about either the y - or z -axis results in 3-D random orientation of the fillers in the matrix. The properties of the mixture of fillers and isotropic matrix rotated by an angle ϕ degree about the y -axis are computed using the transformation matrix [T_y]. The transformed stiffness matrix [C''] has the form of:

$$[C''] = [T_y][\bar{C}'][T_y]^T \tag{14}$$

where [T_y]^T is the transpose matrix of [T_y]. The effective stiffnesses, \bar{C}''_{ij} are obtained by another random rotation along the y -axis:

$$\bar{C}''_{ij} = \frac{1}{\pi} \int_0^\pi C''_{ij} d\phi \tag{15}$$

Now, the components of [\bar{C}''] can be expressed by using C''_{ij} as follows:

$$\begin{aligned}
\bar{C}_{11}'' = \bar{C}_{22}'' &= \frac{1}{512} (195C_{11}^0 + 56C_{12}^0 + 138C_{13}^0 + 123C_{33}^0 + 276C_{44}^0 + 112C_{66}^0) \\
\bar{C}_{12}'' &= \frac{1}{512} (65C_{11}^0 + 104C_{12}^0 + 302C_{13}^0 + 41C_{33}^0 - 164C_{44}^0 - 48C_{66}^0) \\
\bar{C}_{13}'' = \bar{C}_{23}'' &= \frac{1}{128} (15C_{11}^0 + 40C_{12}^0 + 66C_{13}^0 + 7C_{33}^0 - 28C_{44}^0 - 16C_{66}^0) \\
\bar{C}_{33}'' &= \frac{1}{64} (33C_{11}^0 + 8C_{12}^0 + 14C_{13}^0 + 9C_{33}^0 + 28C_{44}^0 + 16C_{66}^0) \\
\bar{C}_{44}'' = \bar{C}_{55}'' &= \frac{1}{128} (15C_{11}^0 - 8C_{12}^0 - 14C_{13}^0 + 7C_{33}^0 + 52C_{44}^0 + 32C_{66}^0) \\
\bar{C}_{66}'' &= \frac{1}{512} (65C_{11}^0 - 24C_{12}^0 - 82C_{13}^0 + 41C_{33}^0 + 220C_{44}^0 + 80C_{66}^0) \\
\bar{C}_{14}'' = \bar{C}_{15}'' = \bar{C}_{16}'' = \bar{C}_{24}'' = \bar{C}_{25}'' = \bar{C}_{26}'' &= 0 \\
\bar{C}_{34}'' = \bar{C}_{35}'' = \bar{C}_{36}'' = \bar{C}_{45}'' = \bar{C}_{46}'' = \bar{C}_{56}'' &= 0
\end{aligned} \tag{16}$$

Since the matrix contains 3-D randomly oriented and evenly distributed fillers, it is presumed to be macroscopically isotropic. Therefore, it must satisfy the following relations numerically.

$$\begin{aligned}
\bar{C}_{11}'' = \bar{C}_{22}'' = \bar{C}_{33}'' \\
\bar{C}_{12}'' = \bar{C}_{13}'' = \bar{C}_{23}'' \\
\bar{C}_{44}'' = \bar{C}_{55}'' = \bar{C}_{66}''
\end{aligned} \tag{17}$$

Extensional and Shear Moduli (Platelet filler model)

The extensional modulus of the mixture of the 3-D randomly oriented platelet clay fillers and matrix, $E_m^{platelet}$ can be obtained from:

$$E_m^{platelet} = \frac{1}{\bar{S}_{11}''} \tag{18}$$

where \bar{S}_{11}'' is a component of compliance matrix. Using the stiffnesses \bar{C}_{ij}'' and the relations in Eq. (17), Eq. (18) can be rewritten in the following form:

$$E_m^{platelet} = \frac{(\bar{C}_{11}'')^3 - 3\bar{C}_{11}''(\bar{C}_{12}'')^2 + 2(\bar{C}_{12}'')^3}{(\bar{C}_{11}'')^2 - (\bar{C}_{12}'')^2} \tag{19}$$

The shear modulus of the mixture of the 3-D randomly oriented platy kaolin clay fillers and matrix, $G_m^{platelet}$ can be computed using;

$$G_m^{platelet} = \bar{C}_{66}'' \tag{20}$$

Equation (20) can be rewritten in terms of engineering properties of the mixture of the unidirectional fillers and the matrix shown in Fig. 2a:

$$\begin{aligned}
G_m^{platelet} &= \frac{20G_{xy}^0 + 55G_{zx}^0}{128} + \frac{41\{1 - (\nu_{xy}^0)^2\}}{512(E_{xx}^0)^2\Delta} \\
&+ \frac{65(1 - \nu_{xz}^0\nu_{zx}^0) - 24(\nu_{xy}^0 + \nu_{xz}^0\nu_{zx}^0) - 85(\nu_{zx}^0 + \nu_{xy}^0\nu_{zx}^0)}{512E_{xx}^0E_{zz}^0\Delta}
\end{aligned} \tag{21}$$

where

$$\Delta = \frac{1 - \nu_{xy}^0\nu_{yx}^0 - 2\nu_{xz}^0\nu_{zx}^0 - 2\nu_{yx}^0\nu_{xz}^0\nu_{zx}^0}{(E_{xx}^0)^2 E_{zz}^0} \tag{22}$$

Estimation of Properties of Composites consisting of roving and CSM layers

Since there are only two types of layers, roving layers and CSM layers as in the composites under consideration, the mechanical properties of composites can be expressed by using the properties of layers [1]:

$$\bar{E}_{11} = \eta_{E_{11}} + \eta_{mat} - \frac{(v_{12/roving}\eta_{E_{22}} + v_{mat}\eta_{mat})^2}{\eta_{E_{22}} + \eta_{mat}} \tag{23}$$

$$\bar{E}_{22} = \eta_{E_{22}} + \eta_{mat} - \frac{(v_{12/roving}\eta_{E_{22}} + v_{mat}\eta_{mat})^2}{\eta_{E_{11}} + \eta_{mat}} \tag{24}$$

$$\bar{G}_{12} = G_{12/roving}v_{roving} + G_{mat}v_{mat} \tag{25}$$

$$\bar{\nu}_{12} = \frac{v_{12/roving}\eta_{E_{22}} + v_{mat}\eta_{mat}}{\eta_{E_{22}} + \eta_{mat}} \tag{26}$$

and

$$\eta_{E_{11}} = \frac{E_{11/roving}v_{roving}}{1 - v_{12/roving}v_{21/roving}}$$

$$\eta_{E_{22}} = \frac{E_{22/roving}v_{roving}}{1 - v_{12/roving}v_{21/roving}} \tag{27}$$

$$\eta_{mat} = \frac{E_{mat}v_{mat}}{1 - v_{mat}^2}$$

where v_{roving} and v_{mat} are the volume fractions of the roving and CSM layers, respectively, satisfying the relation that $v_{roving} + v_{mat} = 1$. $E_{ij/roving}$ and E_{mat} are the extensional moduli of the roving and CSM layers. $G_{12/roving}$ and G_{mat} are the shear moduli of the roving and CSM layers, respectively. $\nu_{ij/roving}$ and ν_{mat} are the

Poisson's ratios of the roving and CSM layers respectively.

EXPERIMENT

Composites Samples

Three groups of pultruded composite material reinforcing schemes have been examined in this study. These are denoted as VG-1, VG-2 and VG-3, and they consist of E-glass roving and CSM layers as shown schematically in Figs. 3, 4 and 5, respectively. Two layers of E-glass Nexus veil are on the top and bottom of the structures. The matrices of these composites are vinylester with clay fillers. The properties of the composite constituents such as E-glass fiber, vinylester resin and clay filler are listed in Table 1.

Table 1. Properties of polymer composite constituents

	Young's modulus GPa (ksi)	Shear modulus GPa (ksi)	Poisson's ratio	Density g/cm ³ (lb/ft ³)
E-glass fiber	72 (10,500)	29 (4,200)	0.25	2.56 (160)
Vinylester resin	3.85 (558)	1.4 (204)	0.37	1.26 (79)
Clay filler	20 (2,900)	7.69 (1,115)	0.30	2.60 (162)

Mass measurements of the fiber and matrix materials of the composites were performed following the procedures described by Ye, et al. [9]. The process of obtaining the volume and volume fraction of each constituent was discussed in detail by Park. Table 2 shows average volumes and volume fractions of the composite constituents of six tested specimens.

Table 2. Average volume fractions of the constituents (6 to 8 samples each)

		VG-1 (6 samples)		VG-2 (6 samples)		VG-3 (8 samples)	
		Avg. (%)	STD (%)	Avg. (%)	STD (%)	Avg. (%)	STD (%)
		Total fibers	v_f	29.2	1.57	33.4	1.95
E-glass roving	$v_{f/roving}$	12.0	0.87	18.3	1.38	17.3	1.14
E-glass CSM	$v_{f/mat}$	17.0	1.15	15.2	0.95	15.7	1.94
Vinylester resin	v_r	58.7	1.20	57.8	1.28	58.3	1.68
Clay filler	v_{filler}	11.1	0.87	8.1	1.23	7.9	0.96
Total voids	v_{void}	0.9	0.29	0.7	0.13	0.8	0.25

Shear Test

An asymmetric four point bending shear fixture and test method [10] were used to obtain shear behaviors of the materials. Six to eight composite coupons of each group were tested. The schematic figure and dimensions

of the coupons are shown in Fig. 6. An MTS 810 tension/compression material test system was used for applying tensile load to the shear fixture at a rate of 0.15 mm/min. The data of the applied load and strains were logged by an Optim Megadac 5180AC system and the scanning interval was 1 second. In a pure shear strain field, the principal strains are along $\pm 45^\circ$ directions to the longitudinal axis. One is a tensile strain and the other is a compressive strain. They are, however, theoretically equal in magnitude.

Two element stacked rosettes (CEA-06-062WT-350) manufactured by Measurement Group were used to measure -45° and $+45^\circ$ directional strains. In order to examine how close the test section (center between two notches) is to the pure shear stress state, strains along the longitudinal direction (x -axis) need to be measured. Therefore, three element stacked rectangular rosettes (WK-13-060WR-350) manufactured by Measurement Group were also selected to measure strains -45° , 0° and $+45^\circ$ oriented to the longitudinal axis (x -axis). The strain rosettes were attached on both sides of the specimen to check twisting and out-of-plane bending. If the twisting or the out-of bending was higher than allowance limit [11], the data from the shear test were discarded. A linear regression method [11] was used to determine the shear modulus from the slope of shear stress-strain curve between 0.1% and 0.6% strain. The number of data points in that range was always greater than 50. Fig. 7 shows failed coupons after shear tests.

COMPARISON

Table 3. Comparison of the experimentally determined and the computed nominal shear moduli using Platelet filler model and Spherical filler model

Specimen Groups	G_{12}^{exp} GPa (ksi)	$G_{12}^{exp} / G_{12}^{computed}$ Platelet filler model		$G_{12}^{exp} / G_{12}^{computed}$ Spherical filler model	
		Chamis*	Halpin-Tsai**	Chamis	Halpin-Tsai
		VG-1	4.6 (662)	1.00	1.00
VG-2	4.5 (656)	0.97	0.98	0.96	0.97
VG-3	4.4 (631)	0.97	0.97	0.94	0.95

* The properties of roving and mat layers were obtained by Chamis model.

** The properties of roving and mat layers were obtained by Halpin-Tsai model.

The experimentally determined shear moduli of the pultruded composites (G_{12}^{exp}) are listed in Table 3. Table 3 also shows the comparison of nominal values of the

experimentally determined shear moduli and the theoretically evaluated shear moduli of three specimen groups obtained by using platelet filler model ($G_{12}^{platelet}$) and spherical filler models ($G_{12}^{spherical}$), respectively. Each group had six to eight specimens. The tables show that the platelet filler models resulted in better agreement with the experiment. The maximum difference between the shear moduli obtained by the two filler models was 2.9%. Although the percent difference is not large, the shear moduli computed by using the prediction models associated with platelet filler model are closer to the experimental results than those from the models associated with spherical filler model. This is because the platelet filler model was formed based on the actual shapes of clay particles. Among the used micromechanical models associated with the platelet filler model, Halpin-Tsai models predicts the closest shear moduli to the experimental results for the three specimen groups. The ratios of experimentally determined and computed shear moduli ($G_{12}^{Exp} / G_{12}^{Computed}$) by the combination of the analytical models are 1.0, 0.98 and 0.97 for VG-1, VG-2 and VG-3, respectively.

CONCLUSIONS

The volume fractions of all constituents including E-glass fibers, vinylester resin, fine clay fillers and voids were carefully obtained for the estimation. Two different analytical formulae that account for the presence of fine clay fillers and voids in the matrix were successfully developed and compared with experimental results. Additional micromechanical models were used to evaluate the mechanical properties of the matrix, and roving and CSM layers. Finally laminate theory was used to combine the properties of layers to obtain the properties of polymer composites. It was observed that the shear moduli of the matrix materials under consideration computed by the two formulae were closed to. The maximum difference was as high as 3.1%.

The shear moduli of three different polymer composites estimated by using the two filler models and the associated micromechanical models were computed. There were certain differences between the two analytical model groups: (1) the combinations of platelet filler model and the three micromechanical models two filler models and (2) the combinations of spherical filler model and the three micromechanical models. The maximum difference between the two analytical model groups was as high as 2.9%. Although the estimated shear moduli from both analytical model groups correlate with the experimentally determined shear moduli, the combination of platelet filler and Halpin-Tsai models produced the closest agreement with the experimentally determined shear moduli of the three specimen groups.

ACKNOWLEDGEMENT

This work was supported by Faculty Research Grant (FRG) of Minnesota State University, Mankato, Minnesota.

REFERENCES

- [1] Park, J. Y. and Zureick, A., 2005 "Effect of filler and void content on mechanical properties of pultruded composite materials under shear loading," *Polymer Composites*, **26**, pp. 181-192.
- [2] Eshelby, J. D., 1957 "The determination of the elastic field of an ellipsoidal inclusion and related problems," *Proc. R. Soc. A* **241**, pp. 376-396.
- [3] Budiansky, B., 1965, "On the elastic moduli of some heterogeneous materials," *Journal of the Mechanics and Physics of Solids*, **13**, pp. 223-227.
- [4] Mori, T. and Tanaka. T, 1973 "Average stress in matrix and average energy of materials with misfitting inclusions," *Act. Metall*, **21**, pp. 571-574.
- [5] Mura, T., 1987, *Micromechanics of Defects in Solids*, Martinus Nijhoff, Boston, MA.
- [6] Kates, H. S. and Milewski, J. V., 1978, *Handbook of Fillers and Reinforcements for Plastics*, Van Nostrand Reinhold, New York, NY.
- [7] Halpin, J. C. and Tsai, S. W., 1969, "Effect of environmental factors on composite materials," Air Force Materials Laboratory Technical Report, AFML-TR67-423.
- [8] ASTM D 792, 1991, "Standard Test Method for Density and Specific Gravity (Relative Density) of Plastics by Displacement," American Society for Testing and Materials, Philadelphia, PA.
- [9] Ye, B. S., Svenson, A. L. and Bank, L. C., 1995, "Mass and volume fraction properties of pultruded glass fiber-reinforced composites," *Composites*, **26**, pp. 725-731.
- [10] Zureick, A., Berghaus, D. G., and Park, J. Y., 1999, *The In-Plane Shear Properties of Pultruded Materials*, FHWA-Report, Georgia Institute of Technology, Georgia, Atlanta, GA.
- [11] ASTM D 5397, 1993, "Standard Test Method for Shear Properties of Composite Materials by the V-Notched Beam Method," American Society for Testing and Materials, Philadelphia, PA.

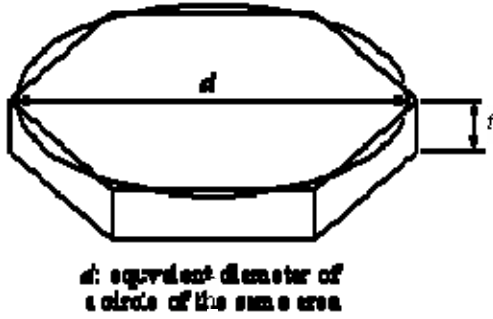


Fig. 1. The schematic shape of the clay particle

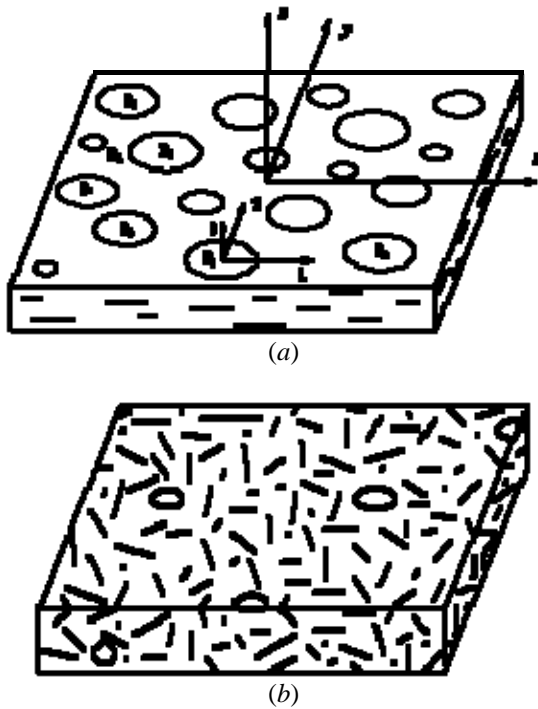


Fig. 2. Platelet filler models: (a) Unidirectional (theoretical) filler model, (b) 3-D random oriented and evenly distributed filler model

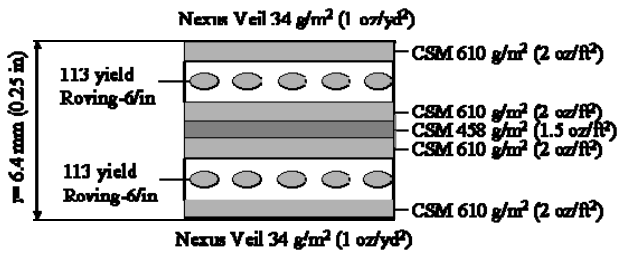


Fig. 3. Schematic figure of stacking sequence of VG-1

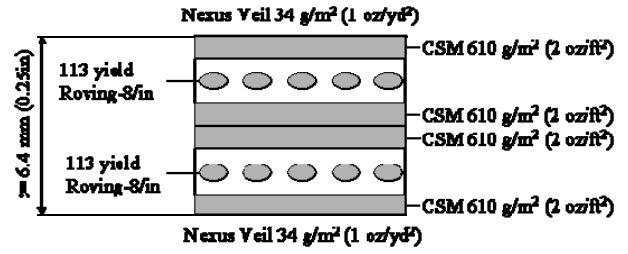


Fig. 4. Schematic figure of stacking sequence of VG-2

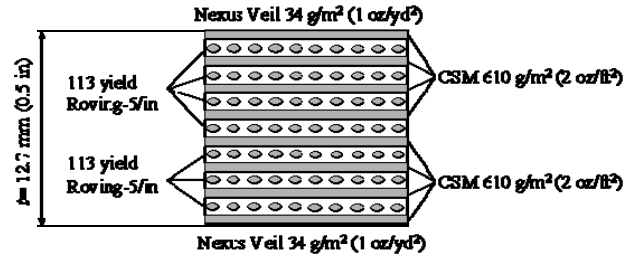


Fig. 5. Schematic figure of stacking sequence of VG-3

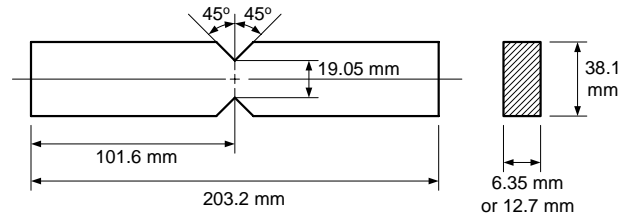


Fig. 6. Schematic figure and dimension of shear test coupon



Fig. 7. A photograph of failed shear test specimen